

RSC Advances



This is an *Accepted Manuscript*, which has been through the Royal Society of Chemistry peer review process and has been accepted for publication.

Accepted Manuscripts are published online shortly after acceptance, before technical editing, formatting and proof reading. Using this free service, authors can make their results available to the community, in citable form, before we publish the edited article. This *Accepted Manuscript* will be replaced by the edited, formatted and paginated article as soon as this is available.

You can find more information about *Accepted Manuscripts* in the [Information for Authors](#).

Please note that technical editing may introduce minor changes to the text and/or graphics, which may alter content. The journal's standard [Terms & Conditions](#) and the [Ethical guidelines](#) still apply. In no event shall the Royal Society of Chemistry be held responsible for any errors or omissions in this *Accepted Manuscript* or any consequences arising from the use of any information it contains.

Synthesis, characterisation and application of imidazolium based ionic liquid modified montmorillonite sorbents for the removal of amaranth dye

Isiaka A. Lawal^a and Brenda Moodley^{a*}

^aSchool of Chemistry and Physics, College of Agriculture, Engineering and Science,
University of KwaZulu-Natal, P/Bag X45001, Westville Campus, Durban, 4000, South
Africa

**corresponding author email: moodleyb3@ukzn.ac.za*

Tel: +27 31 2602796; Fax: +27 31 2603091

First author: lawalishaq000123@yahoo.com

Abstract

The removal of amaranth dye using montmorillonite modified with an ionic liquid (IL) was investigated. An ionic liquid (1-methyl, 3-decahexyl imidazolium) was synthesised, and characterised by nuclear magnetic resonance (^1H and ^{13}C NMR), fourier transform infrared (FT-IR) spectroscopy, high resolution mass spectroscopy (HR-MS) as well as thermal gravimetric analysis and differential thermal (TGA/DCS) analysis. The ionic liquid was thereafter used to modify sodium montmorillonite ($\text{Na}^+\text{-Mt}$) to form a hydrophobic montmorillonite that has a positively charged surface, by adding IL in excess of the cation exchange capacity (CEC) of $\text{Na}^+\text{-Mt}$. Energy dispersive X-ray analyser (EDX) was used to determine the chemical composition of $\text{Na}^+\text{-Mt}$. Modified montmorillonite (Mt-IL) and $\text{Na}^+\text{-Mt}$ was characterised using FT-IR, scanning electron microscopy (SEM), x-ray diffraction (XRD) and Brunauer-Emmett-Teller (BET) method, and used in the adsorption study of an anionic amaranth dye. A higher CEC of the Mt-IL (112 meq/100 g) than $\text{Na}^+\text{-Mt}$ (89 meq/100 g) was observed. The effects of sorbent dosage, dye concentration, solution pH and contact time were investigated in order to determine optimal experimental conditions. Optimum adsorption was obtained at pH 2 and adsorption data was better described by the pseudo-second-order kinetics and Langmuir adsorption isotherm. A maximum adsorption capacity of 263.2 mg/g was calculated. The thermodynamic parameters ΔG° , ΔH° and ΔS° were also investigated at temperatures of 313, 303 and 293 K. Column studies were performed on the modified material and the data generated was applied to the Thomas model where high column adsorption capacities of 393.7, 580.9 and 603.6 mg/g at different concentrations were obtained.

Keywords: Ionic liquid, 1-methyl 3-decahexyl imidazolium, montmorillonite, column studies, adsorption, Amaranth.

1. INTRODUCTION

Montmorillonite has been extensively used for the adsorption of organic compounds.¹⁻³ Recently, research has focused on the modification of montmorillonite using a variety of methods and modifiers. Montmorillonite has been modified using dimethyl dihydrogenated tallow ammonium, ammonium and phosphonium surfactants.^{4, 5} Other modifiers include polypropylene on bentonite,⁶ hexadecyltrimethylammonium (HDTMA) on montmorillonite,

montmorillonite intercalated with cetyltrimethylammonium octadecylamine and cetylpyridinium⁷⁻⁹ among others.

These modifications have been based on the high cation exchange capacity (CEC) of montmorillonite, its swelling capacity and high surface area, all resulting in strong adsorption and adsorption capacities.^{10,11} The aluminosilicate layer of montmorillonite has a ratio of 2:1 type structure, with an octahedral $\text{Al}_{2-3}(\text{OH})_6$ layer.¹² The position of the aluminosilicate results in a weak interaction between adjacent lamellae (Si-O---O-Si). As a result, montmorillonite easily separates and coupled with its high cationic exchange capacity ensures favourable conditions for intercalation reactions. Si^{4+} substituted with Al^{3+} in the tetrahedral layer and Mg^{2+} substituted for Al^{3+} in the octahedral layer results in a net negative charge on the clay surfaces. The deficit in charge is balanced by the exchangeable Na^+ or Ca^{2+} cation in the interlayer.¹⁰ If the inorganic cations of montmorillonite are replaced by large alkyl ammonium ions, the physical properties of the montmorillonite changes and the hydrophilic nature of montmorillonite is converted to a hydrophobic form (organo-montmorillonite).¹³ Organo-montmorillonite has been used for the adsorption of dye,^{14, 15} phenolic compounds and other aromatic compounds¹⁶ as well as pesticides.¹⁷

Ionic liquids (ILs) have recently been used for the modification of montmorillonite¹⁸ and nanoparticles.¹⁹ There is presently limited information on the adsorption of organics (including dye) using IL modified materials. To the best of our knowledge the only reported studies are for the adsorption of reactive red-120 (RR) and 4-(2-pyridylazo) resorcinol (PAR) from aqueous solution by Fe_3O_4 magnetic nanoparticles using ionic liquid as a modifier which was recently studied by Absalan and co workers²⁰ and who reported a significant increase in adsorption capacity. Also, adsorption of folic acid, riboflavin, and ascorbic acid from aqueous samples by Fe_3O_4 magnetic nanoparticles using ionic liquid as modifier was also investigated²¹ but no reports have been reported on IL modified montmorillonite. This lack of research on IL modified montmorillonite for the adsorption of dyes has prompted our investigation into the adsorption behaviour of dyes on IL modified montmorillonite.

They (ILs) are low-melting-point salts and form liquids that consist only of cations and anions. Ionic liquids are often considered as green solvents capable of replacing traditional organic solvents,²² composing of an organic cation and an inorganic anion.²³ The anion

mainly controls their water miscibility²⁴ whereas the length of the alkyl chains of the cations influences all the other properties²⁵ such as the hydrophobicity of the material.

In this work, cationic IL (1-methyl, 3-decahexzyl imidazolium) was synthesised (the choice of 16 carbon atoms was guided by the work of Beall²⁶) and used in modifying montmorillonite which was then used to adsorb anionic amaranth dye. Amaranth is a class of azo dye, which is toxic, and its removal from wastewaters is very important as its presence, even in very low concentration, affects aquatic life and invariably affects the food chain. To the best of our knowledge this is the first report of the use of ionic liquid modified montmorillonite for the adsorption of dye.

2. EXPERIMENTAL SECTION

2.1 Materials

Montmorillonite K 10 powder (CAS Number 1318-93-0) used in the present study was purchased from Sigma Aldrich. Its chemical formula is $\text{Na}_{2/3}\text{Si}_8(\text{Al}_{10/3}\text{Mg}_{2/3})\text{O}_{20}(\text{OH})_4$. Methyl-imidazole, 1-bromodecahexane, montmorillonite, NaCl and amaranth (CAS Number 915-67-3) were purchased from Sigma Aldrich. Double distilled deionized water was used for all sample preparation.

2.2 Apparatus

¹H and ¹³C NMR spectra of the derivatives were recorded on an AVANCE DPX-400 (400 MHz) spectrophotometer (Bruker, U.S.A.) with tetramethylsilane (TMS) as the internal standard. High-resolution mass data were obtained using a Bruker micro TOF-Q II ESI instrument operating at ambient temperature. Thermal gravimetric analysis and differential thermal analysis (TGA-DTA/DSC) (SDT Q 600 V 20.9 Build 20 instrument) was used to measure changes in chemical and physical properties of the material. This was measured as a function of increasing temperature from ambient to 1000 °C (with a constant heating rate of 5 °C/min) under nitrogen atmosphere with a flow rate of 50 mL/min. FT-IR spectra of the IL - sodium montmorillonite (Na⁺-Mt) and sodium montmorillonite modified with 1-methyl, 3-decahexyl imidazolium (Mt-IL) samples were recorded on a Perkin Elmer 100 series FT-IR spectrometer. BET Tri-star II 3020.VI.03 was used to determine the surface area, pore-size, pore volume and pore size distribution. The material was degassed using (Micromeritics vacprep 061, sample degas system) at 90 °C for 1 hr and was increased to 200 °C for 12 hr.

The sample was then analysed by Tri-star II 3020.VI.03 under nitrogen atmosphere at 77 K. The surface morphology of the material was examined by scanning electron microscopy (SEM) using the Leo 435 VP model. Chemical composition analysis of montmorillonite was determined using on a Leo 1450 Scanning Electron Microscope equipped with energy dispersive X-ray analyser (EDX). The interlayer spacing of Na⁺-Mt and Mt-IL was measured by X-ray powder diffraction (XRD, Shimadzu XRD-6000, Japan, Cu K α radiation, 40 kV, 40 mA, Japan), and data were collected for 2 θ ranging from 1.3° to 10° with the scan speed of 1 °/min.

2.3 Preparation of ionic liquid (IL), 1-methyl, 3-decahexyl imidazolium

1-methyl, 3-decahexyl imidazolium is a salt which consists of imidazolium (a five ring compound of two ammonium with one of them a quaternary ammonium) at the centre, a methyl group and decahexyl alkyl chain attached to the ammonium and the quaternary ammonium in the ring respectively. The method used by Dzyuba and Bartsch²⁷ was modified for the synthesis of the salt. An oil bath with a stirred flask containing equimolar amounts of N-imidazole and the primary alkyl bromide (bromodecahexane) was heated at 140 °C for 10-15 min and thereafter cooled. The solution was heated again in the oil-bath at 140 °C for another 10-15 min, followed by drying under vacuum at 100-120 °C to give the desired product, a highly viscous golden liquid that solidified at room temperature.

Table 1 Properties of the surfactant and amaranth used in this study

2.4 Preparation of sodium-montmorillonite (Na⁺-Mt) and modification with IL

Montmorillonite was soaked in deionised water for 24 hr and thereafter centrifuged. The upper layer having very fine clay, was decanted and converted to sodium montmorillonite (Na⁺-Mt) using the method employed by Zaghouane-Boudiaf and Boutahala.¹⁰ Briefly, 10 g of montmorillonite was mixed with 1 M NaCl solution and stirred for 24 hr. Thereafter, it was dialyzed in deionized water until it was free of chloride and dried at 80 °C. Na⁺-Mt was further passed through a 53 μ m sieve allowing for the fine Na⁺-Mt particles to be collected. The cation exchange capacity (CEC) of Na⁺-Mt and Mt-IL were determined using the Gillman and Sumpter method,²⁸ with a CEC value of 89 meq/100 g.

The Na⁺-Mt was then modified by adding IL in excess of the CEC of the clay to form Mt-IL. Newam¹² reported that clay can adsorb more than its CEC and in the work of Xu and Boyd,²⁹

³⁰ addition of an organic cation greater than the CEC of clay, led to the adsorption of the organic cation on the external surface of the material through cation exchange and hydrophobic bonding, which generated positive charges on the surface. The mass of IL required was calculated using the following equation.³¹:

$$mc = f * CEC * X * GMW \dots\dots\dots (1)$$

Where mc is the mass of organic cation required to achieve the desired fraction of CEC (g), f is the fraction of cation-exchange capacity satisfied by the organic cation (no unit), CEC is the cation exchange capacity of the clay (mmol/g clay), X is the mass of clay (g) and GMW is the gram molecular weight of IL (g/mol).

The desired IL was slowly added to the desired mass of Na⁺-Mt dispersed in methanol. The mixture was stirred overnight and the modified montmorillonite was washed several times with double distilled deionized water and thereafter dried in an oven at 100 °C overnight.

2.5 Batch adsorption studies

Adsorption experiments were performed in batch mode to investigate the effects of various process parameters such as pH, adsorbent and initial dye concentrations, contact time, and temperature on Na⁺-Mt and Mt-IL. The effect of dose of the adsorbent was carried out with 0.005 g to 0.1 g in 30 mL of amaranth dye having a concentration of 50 mg/L; subsequent parameters (effect of concentration, pH, and temperature) were carried out using the same concentration and volume as in the case of dose. A blank was also determined under the same conditions but without the adsorbent. The concentration of the dye was always measured before and after the adsorption. All experiments were run for 24 hr, to allow sufficient time for the adsorption to reach equilibrium conditions and were carried out in duplicate.

Adsorption kinetics were determined by analysing the adsorptive uptake of amaranth dye from its aqueous solution of 20 mg/L, 50 mg/L, 100 mg/L and 200 mg/L concentrations at different times. The equilibrium data for developing the isotherms were obtained at different temperatures (20, 30, and 40 °C) by mixing 0.05 g of Mt-IL with amaranth for 36 hr. After equilibrium, the aqueous phase concentration of dye in the solution was determined by a double beam UV-Vis-NIR spectrophotometer (Shimadzu Model UV 3600, Japan) at λ_{\max}

520 nm. The equilibrium adsorption capacity of Mt-IL and Na⁺-IL were calculated from the following relationship:

$$q_e = \frac{C_0 - C_e}{W} V \dots\dots\dots (2)$$

Where q_e is the equilibrium adsorption capacity in (mg/g), C_0 and C_e are the dye concentrations at initial and at equilibrium respectively, in mg/L, V is the volume of solution in (L), and W is the weight of adsorbent in (g).

Adsorption data were fitted to Freundlich,³² Langmuir,³³ Temkin and Dubinin-Raduskevich,³⁴ isotherms. Linear equations of all the applied models are:

$$\text{Langmuir model: } \frac{C_e}{q_e} = \frac{C_e}{q_m} + \frac{1}{q_m b} \dots\dots\dots (3)$$

$$\text{Freundlich model: } \ln q_e = \ln K_f + \frac{1}{n} \ln C_e \dots\dots\dots (4)$$

$$\text{Temkin model: } q_e = B \ln A + B \ln C_e \dots\dots\dots (5)$$

$$\text{Dubinin-Raduskevich model: } \ln q_e = \ln q_m - \beta \Sigma^2 \dots\dots\dots (6)$$

$$\Sigma = RT \ln \left[1 + \frac{1}{C_e} \right] \dots\dots\dots (7)$$

$$E = \frac{1}{\sqrt{2\beta}} \dots\dots\dots (8)$$

Where C_e is the equilibrium dye concentration in the solution in mg/L, b is the Langmuir adsorption constant (L/mg), and q_m is the theoretical maximum adsorption capacity (mg/g). K_f (L/mg) and n are Freundlich isotherm constants indicating the capacity and intensity of the adsorption, respectively. A is the equilibrium binding constant (L/mg) and B is the heat of adsorption. β is the Dubinin-Raduskevich model constant (mol²/kJ²) related to the mean free energy of adsorption per mole of the adsorbate and Σ is the polanyi potential. E is the mean free energy of adsorption (kJ/mol).

In order to determine the mechanism and potential rate-controlling steps involved in the process of adsorption, pseudo first order,³⁵ pseudo second order.³⁶ The pseudo first order kinetic model equation is:

$$\ln (q_e - q_t) = \ln q_e - K_1 t \dots\dots\dots (9)$$

Where q_t is the amount of adsorption at time t in (mg/g), k_1 is the rate constant of the equation in (1/min), and q_e is the amount of adsorption equilibrium in (mg/g). The adsorption rate constant (k_1) can be determined experimentally by plotting $\ln(q_e - q_t)$ versus t .

The pseudo second order kinetic model is expressed as:

$$t/q_t = 1/(k_2 q_e^2) + t/q_e \dots \dots \dots (10)$$

Where k_2 is the equilibrium rate constant of pseudo second order adsorption in (g/mg min). The values of k_2 and q_e can be determined from the slope and intercept of the plot t/q_t versus t , respectively.

The data was also fitted into the Weber–Morris model, to evaluate the possibility of intra-particle diffusion as the rate limiting step; it is given by³⁷:

$$q_t = k_{id} t^{1/2} + C \dots \dots \dots (11)$$

Where k_{id} (mg/g/h^{1/2}) is the intra-particle diffusion rate constant.

2.6 Fixed bed column studies

Fixed bed column studies were conducted using glass columns of 1.5 cm internal diameter and 55 cm length. The column was packed with the modified montmorillonite between two supporting layers of glass wool to prevent the adsorbent floating from the outlet. The mass of the adsorbent and the flow rate (3.2 mL/min) were kept constant while the influent concentration was varied from 50 to 200 ppm. The data was fitted into the Thomas model³⁸ in order to predict the adsorptive curve of breakthrough in a fixed-bed.

The Thomas expression is represented by equation 12:

$$\frac{C_t}{C_0} = \frac{1}{1 + \exp[k_{Th}(q_0 x - C_0 V_{eff})/v]} \dots \dots \dots (12)$$

Where k_{Th} is the Thomas rate constant (mL/min/mg), q_0 is the equilibrium uptake of the dye per g of the adsorbent (mg/g), x represents the mass of adsorbent in the column (g), V_{eff} is the effluent volume (mL), C_0 and C_t is the dye influent concentration and effluent concentration at time t (mg/L) respectively, and v is the flow rate (mL/min). The value of C_t/C_0 is the ratio of effluent and influent of the dye concentrations. The value of time t (min) is $t = V_{eff}/v$. The kinetic coefficient k_{Th} and the adsorption capacity of the column q_0 can be determined from a plot of C_t/C_0 against t at a given flow rate using non-linear regression from equation 13:

$$\ln\left(\frac{C_0}{C_t} - 1\right) = \frac{k_{Th} q_0 X}{v} - k_{Th} C_0 t \dots\dots\dots (13)$$

3. RESULTS AND DISCUSSION

3.1 Characterization of IL, Mt, Na+–Mt and Mt–IL

1H NMR, ^{13}C NMR and FT-IR analyses were carried out and thermal stabilities were confirmed by TGA-DTA/DSC (see supporting information (SI)). 1H NMR of IL (400 MHz, $CDCl_3$): δ (ppm) 0.81 (t, 3H), 1.2 (m, 26H), 1.8 (q, 2H), 4.0 (s, 3H), 4.2 (t, 2H), 7.4 (d, 1H), 7.5 (d, 1H) and 10.2 (s, 1H). ^{13}C NMR of IL (400 MHz, $CDCl_3$) at δ (ppm): 14.1, 22.7, 26.3, 29.0, 29.3, 29.4, 29.5, 29.58, 29.6, 29.7, 30.3, 31.9, 36.7, 50.2, 121.7, 121.5, and 137.6). FT-IR of IL $\nu = 3477$ and 3430 (N–H stretch, 2° amines), 3145 , 3083 and 3063 (C–H stretch, aromatics), 2950 , 2915 , 2850 (C–H stretch, alkanes), 2051 , 1631 , 1573 (C–C stretch (in-ring), aromatics), 1473 , 1427 (C–H bend, alkanes), 1381 , 1343 , 1313 (C–H rocking, alkanes), 1175 (C–N stretch, aromatic amines), 1022 , 862 , 792 , 739 , 716 , 662 , 623 , 512 , 481 , 434 , 401 (C–H aromatics).

High-resolution mass spectroscopy was used to confirm the mass of the IL. The result of the HRMS is as follows: HRMS of $[C_{20}H_{13}N_2]^+$ (m/z): 307.3110; calculated mass is 307.3113 g/mol (see SI for the HRMS spectra). Thermogravimetric analysis (TGA) showed that the ionic liquid is thermally stable up to 350 °C (additional spectral data can be found in the supporting information). Other properties are shown in Table 1.

3.2 Chemical composition of montmorillonite

EDX analysis was used in determining the chemical composition of Na⁺-Mt. Table 2 indicates that silica and alumina are the main components of the Na⁺-Mt, with others such as sodium, potassium, iron, magnesium, and calcium in trace amounts. SiO₂ and Al₂O₃ will be the main adsorbing site.³⁹

Table 2 showing the chemical composition of montmorillonite

Fig. 1a and 1b showing the XRD of Na⁺-Mt, Mt-IL and Mt-IL after adsorption of dye

The XRD of Na⁺-Mt was compared with IL intercalated montmorillonite (Mt-IL) as shown in Figs. 1a and 1b. IL intercalation of the Mt has decreased the intensity of the spectra compared to the unmodified and made the width of the peak at half-peak height broader, suggesting that IL intercalation caused extensive delamination.⁴⁰⁻⁴² A similar result has been reported by Lee and Kim.⁴³ Also the peaks at 001, 002 and 020 reflect at 9.53 Å, 4.87 Å and 4.18 Å, respectively which are an integral part of montmorillonite, and the sharp reflection at the 2θ value of 27.15 (3.28 Å) corresponds to quartz in Na⁺-Mt.¹⁸ When no water molecules are intercalated between the unit layers of montmorillonite the interlayer distance is at (001) and reflection around 9.53 Å.⁴⁴ When intercalation of IL in the interlayer of Na⁺-Mt occurs, 001, 002 and 020 reflections shift to 11.65, 6.24, and 4.79 Å respectively. A similar trend had been reported by Singla and co-workers and Takahashi and co-workers.^{5, 18} IL does not show any XRD peak due to its liquid nature. Furthermore, comparing Na⁺-Mt with Mt-IL, the (001) d-spacing value increases from 9.53 to 11.65 Å and signifies the intercalation of IL in Mt-IL (crystalline swelling). Fig 1c shows that the intensity of all the peaks in the Mt-IL spectrum after adsorption of amaranth dye has increased significantly compared to Mt-IL before adsorption. This suggests that the amaranth dye has been intercalated along with IL already within the Mt.

To ascertain that IL in excess of CEC of Na⁺-Mt is arranged in the silicate layer of Na⁺-Mt, the cation exchangeable capacity of Mt-IL was determined to be 112 meq/100 g. Comparing the CEC with that of Na⁺-Mt (89 meq/100 g), it shows that all exchangeable cations present in the Na⁺-Mt had been exchanged in excess for IL, indicating 125% increase of the Na⁺-Mt CEC resulting in an aggregation on the surface of the clay and an overall positive surface.

Takahashi and co-workers have also reported the intercalation of ionic liquid in the interlayer of montmorillonite.¹⁸ To further ascertain that quaternary ammonium cations in 1-methyl, 3-decahexyl imidazolium were intercalated into the silicate lattice of Na⁺-Mt, FT-IR of the pure montmorillonite, Na⁺-Mt and Mt-IL spectra were recorded in the region 380–4000 cm⁻¹ as shown in Fig. 2.

Fig 2. FT-IR spectra of Mt, Na⁺-Mt and Mt-IL

The presence of peaks in the region of 3392-3314 and 1639 cm⁻¹, represent the stretching and bending modes respectively of the -OH of water within the montmorillonite.⁷ It is observed that the 3314 cm⁻¹ band intensity on Mt-IL decreases when compared with Na⁺-Mt which implies that water of hydration is lost as the cation (Na⁺) is replaced by the cationic surfactant (alkyl chain). A similar result was also reported by Zaghouane-Boudiaf and Boutahala.¹⁰ The peaks at 2920 and 2851 cm⁻¹ are assigned to symmetric and asymmetric stretching vibrations of the methylene groups in the ionic liquid while peaks 1573 and 1467 cm⁻¹ are their bending vibrations respectively,⁴⁵ showing the intercalation of ionic liquid molecules between the silica layers. These peaks were not present in the unmodified montmorillonite. The peaks at 1029 and 459 cm⁻¹ are the bands for Si-O-Si stretching and bending respectively.⁴⁶⁻⁴⁹ There is little difference between the spectra for Mt-IL before after adsorption of amaranth dye (Mt-IL-amaranth). There was a slight shift in the peaks after adsorption of dye from 2921.70 and 2852.30 cm⁻¹ to 2919.60 and 2851.87 cm⁻¹ (symmetric and asymmetric stretching vibrations of the methylene groups), also from 1574.73 and 1467.42 cm⁻¹ to 1573.37 and 1468.12 cm⁻¹ (bending vibrations of the methylene groups) respectively. The presence of the OH peak is noticed after adsorption of dye signifying presence of water in the interlayer of Mt (3341.31 cm⁻¹).

The surface morphologies of the Na⁺-Mt and Mt-IL samples are analysed by SEM, with Mt-IL in Fig 3b showing more porosity and irregularity than Na⁺-Mt in Fig. 3a. The modified montmorillonite is slightly expanded, which indicates delamination of the layers of the montmorillonite due to the presence of cations of the salt.⁵⁰ Fig. 3a (Na⁺-Mt) also shows a clump like morphology with smooth surface as compared with Fig. 3b that shows agglomerated sheet like morphological characteristic with rough surface. Similar results have been reported by Anggraini and co-workers.⁵¹ Fig. 3c shows the morphology of the Mt-IL after adsorption and indicates that the adsorbed dye has blocked the pores of the material.

Fig 3. SEM images of Na⁺-Mt (a) and Mt-IL (b) before adsorption and after adsorption (c)

Fig. 4a shows the N₂ adsorption desorption isotherm of Na⁺-Mt, where the material exhibited a type IV isotherm which is a characteristic of mesoporous material according to IUPAC classification (material having pores ranging from 1.5-100 nm).⁵² The adsorbent also showed a H₃ hysteresis loop over the range of relative pressure P/P₀ 0.40 - 1.00 which signifies that the material has pore blocking (forming slit shaped pores) with non-uniform pore size distribution and shape. The average pore diameter of the sample was within the mesoporous and macroporous range, with most of it being mesoporous. In Fig. 4b Na⁺-Mt shows narrow pore size distribution with most pores centred at about 7.62 nm and a very broad range of pores from 7.62-249 nm.

The surface area of Na⁺-Mt was 183.2 m²/g and with a pore volume of 0.52 cm³/g. There is a decrease in the surface area (175 m²/g) and pore volume (0.32 cm³/g) for Mt-IL, which is due to blocking of the pores by the ionic liquid cations. Also, Mt-IL in Figs. 5a and 5b also showed a type IV isotherm and H₃ hysteresis, but due to the modification by 1-methyl, 3-decahexyl imidazolium, the pore size has increased and is more macroporous than mesoporous.

Figs. 4a and 4b. N₂ adsorption desorption isotherm and pore size distribution of Na-Mt respectively.

Figs. 5a and 5b. N₂ adsorption desorption isotherm and pore size distribution of Mt-IL respectively.

The thermal study of the material shows loss of water observed in the Mt-IL TG-DTA spectra (see SI) which is due to the removal of the externally adsorbed and interlayer water at about 100 °C. The decomposition of the IL was observed in the range of 300 to 450 °C and an endothermic peak is observed around 700 °C which corresponds to the decomposition of the structural hydroxyl groups in the aluminosilicate.^{18, 53}

3.3 Batch Adsorption

The effect of amaranth on Na⁺-Mt and Mt-IL doses from 0.005-0.1 g was carried out and showed an increase in adsorption of amaranth on Na⁺-Mt and Mt-IL as their masses increased. This could be attributed to electrostatic attraction between the amaranth dye ion and the positively charged surface of the materials (Na⁺-Mt and Mt-IL). Interaction between the rings on the amaranth dye molecule and the Mt-IL may also occur ($\pi - \pi$ interaction). Adsorption reached its maximum at about 0.01 g with 90% of the dye adsorbed (Fig. 6a). It was also observed that after adsorption reached equilibrium, the adsorbed dye showed a continuous decline as the amount of sorbent increased. Daneshvar and Ghosh,^{54, 55} reported the same trend⁵⁴ and suggested that it was as a result of increasing particle interaction and aggregation, leading to a reduction of total surface area. On the other hand, there is a gradual increase in the percentage removal of amaranth dye as the mass of Na⁺-Mt increases which is due to the increase in surface area with a high dosage of the adsorbent. Na⁺-Mt could adsorb about 30% at 0.1 g which could be attributed to fewer adsorption sites and lack of electrostatic interaction⁵⁶ between amaranth dye and Na⁺-Mt. Since the optimized dose is 0.01 g for Mt-IL, all other optimization experiments were performed with 0.01 g of sorbent.

The effect of pH showed that maximum adsorption was at pH 2, and decreases gradually as the pH tends towards basic medium (Fig. 6b). Other researchers reported similar trends for adsorption of anionic dye.^{39, 57} This can be explained by electrostatic attraction between the negatively charged adsorbate and positively charged adsorbent. At low pH levels a positively charged ion dominates the surface of the adsorbent because of the activities of the functional group on the adsorbent and the presence of IL in excess on the adsorbent. Amaranth is an anionic dye with predominantly negative charges at low pH. This negative charge on the dye at low pH results in a significantly high electrostatic attraction between the positive and negative charges on the adsorbent and the dye respectively.^{57, 58} Therefore, an increase in adsorption of the dye will occur at the Mt-IL surface. When pH is increased there will be more negative ions on the surface of the adsorbent, causing repulsion which will reduce adsorption. Also, at higher pH values excess of OH⁻ is present in the solution, which can lead to competition of adsorption sites with amaranth ions. Nevertheless, there is still significant amount of dye adsorbed onto Mt-IL at higher pH values. This can be attributed to chemisorption,³⁹ i.e. chemical reaction between the adsorbent aromatic ring and the ring of the amaranth dye. All other experiments were carried out on Mt-IL only at pH of approximately 2. The adsorption capacity of Na⁺-Mt (6 mg/g) is much lower than Mt-IL.

Figs. 6a and 6b, showing the effect of dose of adsorbent and pH respectively.

3.4 Adsorption Kinetics of Amaranth

The effect of contact time on the extent of amaranth adsorption of different concentrations in the plot of removal efficiency against time as shown in Fig. 7 indicated that the adsorption of amaranth on the adsorbent increased with time. Equilibrium time for 20 mg/L, 50 mg/L, 100 mg/L and 200 mg/L was about 120 min. Ahmad, also reported equilibrium times of 120 min for amaranth onto alumina reinforced polystyrene.⁵⁷

It was also observed that the adsorption of amaranth is very rapid in the first 10 min at all concentrations but later decreased with time until equilibrium was reached. A large number of free adsorbent sites available for sorption are likely to be responsible for the high removal of the amaranth dye at the beginning of the experiment. The decrease in adsorption rate was as a result of a reduction in available sites and also because of repulsive forces among adsorbed dye molecules and unmodified adsorption sites present in the solution.⁵⁹

Fig 7. Plot of removal efficiency % against time (min) for four different concentrations at pH 2

To have a better understanding of the adsorption kinetics, mechanism and the potential rate-controlling step involved in the process of adsorption, several kinetic models were used. These include Lagergren-first-order model, pseudo-second-order kinetic model and intra-particle diffusion. Table 3 showed that pseudo-second-order fitted best with $R^2 \geq 0.99$ for all the concentrations at different temperatures. From the result in the above models, amaranth adsorption on to Mt-IL was most probably chemisorption and took place through exchange of ions on the surface of the active sites which is in agreement with other studies.^{57, 60-62} Also, the adsorption capacity (q_e) calculated for all the concentrations were very close to q_e experimental as shown in Table 3. Similar results were reported by Ahmad and Zargar.^{57, 63, 64} According to Ho and co-workers and Liao and co-workers,^{36, 61} three steps were involved in the pseudo second order kinetic model, which are: (i) the dye molecules diffuse from liquid phase to liquid–solid interface; (ii) the dye molecules move from liquid–solid interface to solid surface; and (iii) the dye molecules diffuse into the particle pores.

The data were further fitted into the intra-particle diffusion model to examine the relative contribution of surface and intra-particle diffusion to the kinetics process. The plot not passing through the origin indicated some degree of boundary layer control which further showed that the intra-particle diffusion was not the only rate controlling step, but other processes also controlled the rate of adsorption.^{57, 61, 65} Surface diffusion mechanism is likely attributed to electrostatic attraction, since amaranth will be negatively charged at pH 2 and the surface of the material is positivity charged.

Table 3 Experimental values for q_e (mg/L) and parameters for pseudo-first-order, pseudo-second-order and intra-particle diffusion.

Table 4 The q_m and b values in Langmuir equation, the K_f and $1/n$ values in Freundlich equation, q_s and β values in Dubinin-Radushkevich, bT and AT values in Temkin models and their respective correlation coefficients values.

Table 4 showed that Langmuir was best fitted for the data with $R^2 > 0.99$ for all the temperatures. This further confirmed the previous statement that the adsorption process of the dye onto Mt-IL was chemisorbed onto its surface. The Langmuir isotherm fitted the experimental data for all the temperatures very well, which implied that the active sites on Mt-IL were homogeneously distributed, since the Langmuir equation assumed that the surface was homogeneous. Furthermore, the maximum sorption capacities (q_m) were 243.902, 238.095 and 263.158 mg/g at temperatures 313 K, 303 K and 313 K respectively, and it was concluded that Langmuir is the best fit isotherm. To the best of the authors' knowledge the adsorption capacity is high compared with other previous research carried out on amaranth which the authors attribute to the ionic liquid used in the modification of the montmorillonite. Also, from Dubinin-Radushkevich the mean sorption energy (E) derived from the D-R isotherm model can be used to distinguish chemical and physical adsorption. Table 4 showed E values of 10.00, 7.91 and 8.34 kJ/mol, which were in the range of 8–16 kJ/mol which suggested a dominating chemisorption⁶⁶ effect which is in agreement with other kinetics models. This is also evident in the XRD studies (Fig. 1c) where the intensity of the peaks increased which suggested a chemical reaction between IL on the Mt and the amaranth dye after adsorption.

Thermodynamic studies showed negative values of ΔG at temperatures 313, 303 and 293 K. The values of ΔH , ΔS and the R^2 are listed in the supplemental information. The positive value of ΔH indicated that the adsorption process was endothermic in nature and the positive value of ΔS may be due to the increase in the dye concentration at the solid phase.^{57, 67-70} The negative values of ΔG showed that the process was thermodynamically feasible and spontaneous. This is similar to reports by other researchers.^{55, 57, 68}

Table 5 Comparison of adsorption capacities of Mt-IL with other adsorbents of amaranth dye

Table 5 indicates that the adsorption capacities obtained from this study were far higher having a q_e value (263.20 mg/g) compared to that reported in previous literature for the adsorption of amaranth dye from other adsorbents.

3.5 Column studies

The effect of different concentrations from 50 to 200 mg/L of amaranth dye influent with a constant mass of Mt-IL and constant solution flow rate of 3.2 mL/min is shown in the breakthrough curve in Fig. 8. Fig. 8 showed increased breakthrough times with decreased influent concentrations of amaranth dye and steeper breakthrough curves at increased influent concentrations. The reason for this is because at higher influent concentrations, transportation of amaranth dye to the adsorbent is faster because of an increased diffusion coefficient or mass transfer coefficient which is the driving force for the adsorption process.⁷⁶ As a result this leads to higher gradients of the breakthrough curves at increased concentrations. The larger the influent concentration, the steeper the slope of the breakthrough curve and the shorter the breakthrough time.⁷⁷ These results also showed that a change in concentration of influent affects the saturation rate, and implies that the diffusion process is concentration dependent. Similar trends were obtained from other work.⁷⁸⁻⁸⁰

The column data were fitted into the Thomas model to determine the Thomas rate constant k_{Th} , and equilibrium uptake of amaranth dye per gram of the adsorbent (mg/g) q_0 . Table 6 showed the parameters of the Thomas model, with R^2 values ranging from 0.941 to 0.998. This showed that the Thomas model is suitable for the adsorption of amaranth on Mt-IL. Also, from Table 6, as the influent concentration increased the value of column adsorption capacity q_0 increased (393.63, 580.89 and 603.60 mg/g at 50, 100 and 200 mg/L

respectively). The increased concentrations of solute in solution resulted in increased rates of transportation of solutes to the adsorbent thus leading to increased adsorption capacities.^{77, 79, 81} Thus column studies also confirmed the high adsorption capacity of IL modified montmorillonite for the adsorption of amaranth dye.

Table 6 Thomas model parameters at different concentrations using non-linear regression analysis

Fig. 8 Breakthrough curves showing the effect of influent concentration on amaranth dye

4. CONCLUSION

In this study, a novel, cationic ionic liquid was synthesized for the modification of sodium-montmorillonite. The modified material is hydrophobic with a large pore volume to trap pollutants and is a mixture of mesoporous and macroporous. Adsorption of Mt-IL studies showed that 1-methyl, 3-decahexyl imidazolium intercalated in the interlayer of montmorillonite is a possible good alternative for the removal of anionic amaranth dye from wastewater. The maximum removal percentage was > 90% at an optimum pH of 2. The adsorption behaviour was best described by the Langmuir isotherm with a high adsorption capacity of 263.2 mg/g and the kinetics by pseudo-second-order. Positive values of enthalpy change suggested the endothermic nature of the process, while the negative free energy proved its thermodynamic feasibility and spontaneity. Column experiments using the Thomas model also showed high adsorption capacities of 393.64, 580.89 and 603.60 mg/g at different concentrations. From the result in this research, ionic liquid modified montmorillonite is a good alternative for adsorption of dye from wastewater.

Acknowledgments

The authors wish to acknowledge the University of KwaZulu-Natal for the use of the instrumentation in this study.

REFERENCES

1. D. Avisar, O. Primor, I. Gozlan and H. Mamane, *Water, Air, & Soil Pollution*, 2010, **209**, 439-450.
2. A. Meleshyn and D. Tunega, *Geoderma*, 2011, **169**, 41-46.
3. Q. Wu, Z. Li and H. Hong, *Applied Clay Science*, 2013, **74**, 66-73.
4. D. L. Ho, R. M. Briber and C. J. Glinka, *Chemistry of Materials*, 2001, **13**, 1923-1931.
5. P. Singla, R. Mehta and S. N. Upadhyay, *Green and Sustainable Chemistry*, 2012, **2**, 21-25.
6. B. Du, Z. Guo, P. a. Song, H. Liu, Z. Fang and Y. Wu, *Applied Clay Science*, 2009, **45**, 178-184.
7. M. Boufatit, H. Ait-Amar and W. Mc Whinnie, *Desalination*, 2008, **223**, 366-374.
8. M. Pospíšil, P. Čapková, Z. Weiss, Z. Maláč and J. Šimoník, *Journal of Colloid and Interface Science*, 2002, **245**, 126-132.
9. M. Pospíšil, P. Čapková, D. Měřinská, Z. Maláč and J. Šimoník, *Journal of Colloid and Interface Science*, 2001, **236**, 127-131.
10. H. Zaghouane-Boudiaf and M. Boutahala, *Advanced Powder Technology*, 2011, **22**, 735-740.
11. F.-C. Huang, J.-F. Lee, C.-K. Lee and H.-P. Chao, *Colloids and Surfaces A: Physicochemical and Engineering Aspects*, 2004, **239**, 41-47.
12. A. C. Newman, *Chemistry of Clays and Clay Minerals*, Longman scientific and technical, 1987.
13. S. Y. Lee and S. J. Kim, *Clays and Clay Minerals*, 2002, **50**, 435-445.
14. S. H. Lee, D. I. Song and Y. W. Jeon, *Environmental Technology*, 2001, **22**, 247-254.

15. M. Vakili, M. Rafatullah, B. Salamatinia, A. Z. Abdullah, M. H. Ibrahim, K. B. Tan, Z. Gholami and P. Amouzgar, *Carbohydrate Polymers*, 2014, **113**, 115-130.
16. R. Upson and S. Burns, *Journal of Colloid and Interface Science*, 2006, **297**, 70-76.
17. Y. Hsu, M. Wang, C. Pai and Y. Wang, *Applied Clay Science*, 2000, **16**, 147-159.
18. C. Takahashi, T. Shirai, Y. Hayashi and M. Fuji, *Solid State Ionics*, 2013, **241**, 53-61.
19. H. Sajjadi, A. Modaressi, P. Magri, U. Domańska, M. Sindt, J.-L. Mieloszynski, F. Mutelet and M. Rogalski, *Journal of Molecular Liquids*, 2013, **186**, 1-6.
20. G. Absalan, M. Asadi, S. Kamran, L. Sheikhan and D. M. Goltz, *Journal of Hazardous Materials*, 2011, **192**, 476-484.
21. S. Kamran, M. Asadi and G. Absalan, *Analytical Methods*, 2014, **6**, 798-806.
22. T. Welton, *Chemical Reviews*, 1999, **99**, 2071-2084.
23. E. A. Turner, C. C. Pye and R. D. Singer, *The Journal of Physical Chemistry A*, 2003, **107**, 2277-2288.
24. J. G. Huddleston, A. E. Visser, W. M. Reichert, H. D. Willauer, G. A. Broker and R. D. Rogers, *Green Chemistry*, 2001, **3**, 156-164.
25. A. Jess, A. Große Böwing and P. Wasserscheid, *Chemie Ingenieur Technik*, 2005, **77**, 1430-1439.
26. 4,517,094, 1985.
27. S. V. Dzyuba and R. A. Bartsch, *Journal of Heterocyclic Chemistry*, 2001, **38**, 265-268.
28. G. Gillman and E. Sumpter, *Soil Research*, 1986, **24**, 61-66.
29. S. Xu and S. A. Boyd, *Environmental Science & Technology*, 1995, **29**, 312-320.
30. H. Zhao, W. F. Jaynes and G. F. Vance, *Chemosphere*, 1996, **33**, 2089-2100.

31. N. M. Soule and S. E. Burns, *Journal of Geotechnical and Geoenvironmental Engineering*, 2001, **127**, 363-370.
32. H. Freundlich, *Zeitschrift für Physikalische Chemie*, 1906, **57**, 385-470.
33. I. Langmuir, *Journal of the American Chemical Society*, 1916, **38**, 2221-2295.
34. M. Dubinin and L. Radushkevich, *Chemisches Zentralblatt*, 1947, **1**, 875.
35. S. Lagergren, *Kungliga Svenska Vetenskapsakademiens Handlingar*, 1898, **24**, 1-39.
36. Y.-S. Ho and G. McKay, *Process Biochemistry*, 1999, **34**, 451-465.
37. W. J. Weber and J. C. Morris, *Journal of the Sanitary Engineering Division. ASCE*, 1963, **89**, 31.
38. H. C. Thomas, *Journal of the American Chemical Society*, 1944, **66**, 1664-1666.
39. A. S. Özcan, B. Erdem and A. Özcan, *Journal of Colloid and Interface Science*, 2004, **280**, 44-54.
40. Z. Li, P.-H. Chang, J.-S. Jean, W.-T. Jiang and C.-J. Wang, *Journal of Colloid and Interface Science*, 2010, **341**, 311-319.
41. P. Kulshrestha, R. F. Giese and D. S. Aga, *Environmental Science & Technology*, 2004, **38**, 4097-4105.
42. L. S. Porubcan, C. J. Serna, J. L. White and S. L. Hem, *Journal of Pharmaceutical Sciences*, 1978, **67**, 1081-1087.
43. S. Y. Lee and S. J. Kim, *Journal of Colloid and Interface Science*, 2002, **248**, 231-238.
44. R. E. Grim, *Clay Mineralogy*, McGraw-Hill, New York, 1953.
45. Q. Zhou, R. L. Frost, H. He, Y. Xi and H. Liu, *Journal of Colloid and Interface Science*, 2007, **307**, 357-363.
46. F. Adam, J. N. Appaturi, Z. Khanam, R. Thankappan and M. A. M. Nawi, *Applied Surface Science*, 2013, **264**, 718-726.

47. S. Endud and K.-L. Wong, *Microporous and Mesoporous Materials*, 2007, **101**, 256-263.
48. C. E. A. Kirschhock, R. Ravishankar, F. Verspeurt, P. J. Grobet, P. A. Jacobs and J. A. Martens, *The Journal of Physical Chemistry B*, 1999, **103**, 4965-4971.
49. E. M. Flanigen, H. Khatami and H. A. Szymanski, in *Molecular Sieve Zeolites-I*, ed. F. Gould Robert, American Chemical Society, Washington, DC, 1974, vol. 101, pp. i-iv.
50. O. A. A. dos Santos, C. Z. Castellib, M. F. Oliveirab, A. F. de Almeida Netob and M. G. da Silvab, *Chemical Engineering*, 2013, **32**, 307-312.
51. M. Anggraini, A. Kurniawan, L. K. Ong, M. A. Martin, J.-C. Liu, F. E. Soetaredjo, N. Indraswati and S. Ismadji, *RSC Advances*, 2014, **4**, 16298-16311.
52. T. Allen, *Particle Size Measurement: Volume 2: Surface Area and Pore Size Determination*, Springer, London, 5th edn., 1997.
53. T. Bastow, S. Hardin and T. Turney, *Journal of Materials Science*, 1991, **26**, 1443-1453.
54. E. Daneshvar, M. Kousha, M. S. Sohrabi, A. Khataee and A. Converti, *Chemical Engineering Journal*, 2012, **195–196**, 297-306.
55. D. Ghosh and K. G. Bhattacharyya, *Applied Clay Science*, 2002, **20**, 295-300.
56. H. Yoshida, A. Okamoto and T. Kataoka, *Chemical Engineering Science*, 1993, **48**, 2267-2272.
57. R. Ahmad and R. Kumar, *Clean–Soil, Air, Water*, 2011, **39**, 74-82.
58. P. Baskaralingam, M. Pulikesi, D. Elango, V. Ramamurthi and S. Sivanesan, *Journal of Hazardous Materials*, 2006, **128**, 138-144.
59. C. Smaranda, D. Bulgariu and M. Gavrilesu, *Environmental Engineering and Management Journal*, 2009, **8**, 1391-1402.
60. Y.-S. Ho and G. McKay, *Chemical Engineering Journal*, 1998, **70**, 115-124.

61. P. Liao, Z. Zhan, J. Dai, X. Wu, W. Zhang, K. Wang and S. Yuan, *Chemical Engineering Journal*, 2013, **228**, 496–505.
62. X.-E. Shen, X.-Q. Shan, D.-M. Dong, X.-Y. Hua and G. Owens, *Journal of Colloid and Interface Science*, 2009, **330**, 1-8.
63. B. Zargar, H. Parham and A. Hatamie, *Chemosphere*, 2009, **76**, 554-557.
64. A. Mittal and V. K. Gupta, *Journal of Hazardous Materials*, 2005, **117**, 171-178.
65. G. Crini, H. N. Peindy, F. Gimbert and C. Robert, *Separation and Purification Technology*, 2007, **53**, 97-110.
66. F. G. Helfferich, *Ion exchange*, Courier Dover Publications, 1962.
67. V. Gupta, A. Mittal, V. Gajbe and J. Mittal, *Industrial & Engineering Chemistry Research*, 2006, **45**, 1446-1453.
68. P. Liao, Z. Malik Ismael, W. Zhang, S. Yuan, M. Tong, K. Wang and J. Bao, *Chemical Engineering Journal*, 2012, **195**, 339-346.
69. A. Bhatnagar and A. Jain, *Journal of Colloid and Interface Science*, 2005, **281**, 49-55.
70. S.-H. Lin and R.-S. Juang, *Journal of Environmental Management*, 2009, **90**, 1336-1349.
71. R. Gong, Y. Ding, M. Li, C. Yang, H. Liu and Y. Sun, *Dyes and Pigments*, 2005, **64**, 187-192.
72. R. Jain and S. Sikarwar, *Desalination and Water Treatment*, 2011, **28**, 120-129.
73. H. a. A. Ali, H. a. K. Egzar, N. M. Kamal, N. abdulsaheb and M. S. Mashkour, *International Journal of Basic & Applied Sciences*, 2013, **13**, 57-64.
74. A. Naidu, *Journal of Biochemical Technology*, 2014, **3**, S189-S192.
75. J.-J. Lee, *Clean Technology*, 2011, **17**, 97-102.
76. I. A. W. Tan, A. L. Ahmad and B. H. Hameed, *Desalination*, 2008, **225**, 13-28.

77. Z. Aksu and F. Gönen, *Process Biochemistry*, 2004, **39**, 599-613.
78. R. Han, Y. Wang, W. Yu, W. Zou, J. Shi and H. Liu, *Journal of Hazardous Materials*, 2007, **141**, 713-718.
79. A. Ahmad and B. Hameed, *Journal of Hazardous Materials*, 2010, **175**, 298-303.
80. S.-H. Lin, R.-S. Juang and Y.-H. Wang, *Journal of Hazardous Materials*, 2004, **113**, 195-200.
81. K. Vijayaraghavan, J. Jegan, K. Palanivelu and M. Velan, *Journal of Hazardous Materials*, 2004, **113**, 223-230.

Graphs and Tables

Table 1 Properties of the surfactant and amaranth used in this study

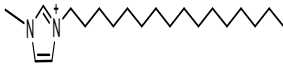
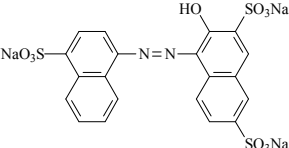
| Compound | Formula | Structure | Molecular Weight (M.W.) g/mol | Appearance | Melting point (°C) |
|-----------------------------------|--------------------------------|---|-------------------------------|----------------------------------|--------------------|
| 1-methyl, 3-decahexyl imidazolium | $C_{20}H_{39}N_2^+$ |  | 307.311 | Golden/solid at room temperature | 62-64 |
| Amaranth | $C_{20}H_{11}N_2Na_3O_{10}S_3$ |  | 604.473 | Powder/Dark red | 120 |

Table 2 showing the chemical composition of montmorillonite

| Constituent | % weight |
|--------------------------------|----------|
| SiO ₂ | 63.51 |
| Al ₂ O ₃ | 21.9 |
| Na ₂ O | 4.11 |
| Fe ₂ O ₃ | 3.1 |
| CaO | 3.22 |
| K ₂ O | 2.1 |
| MgO | 2.06 |

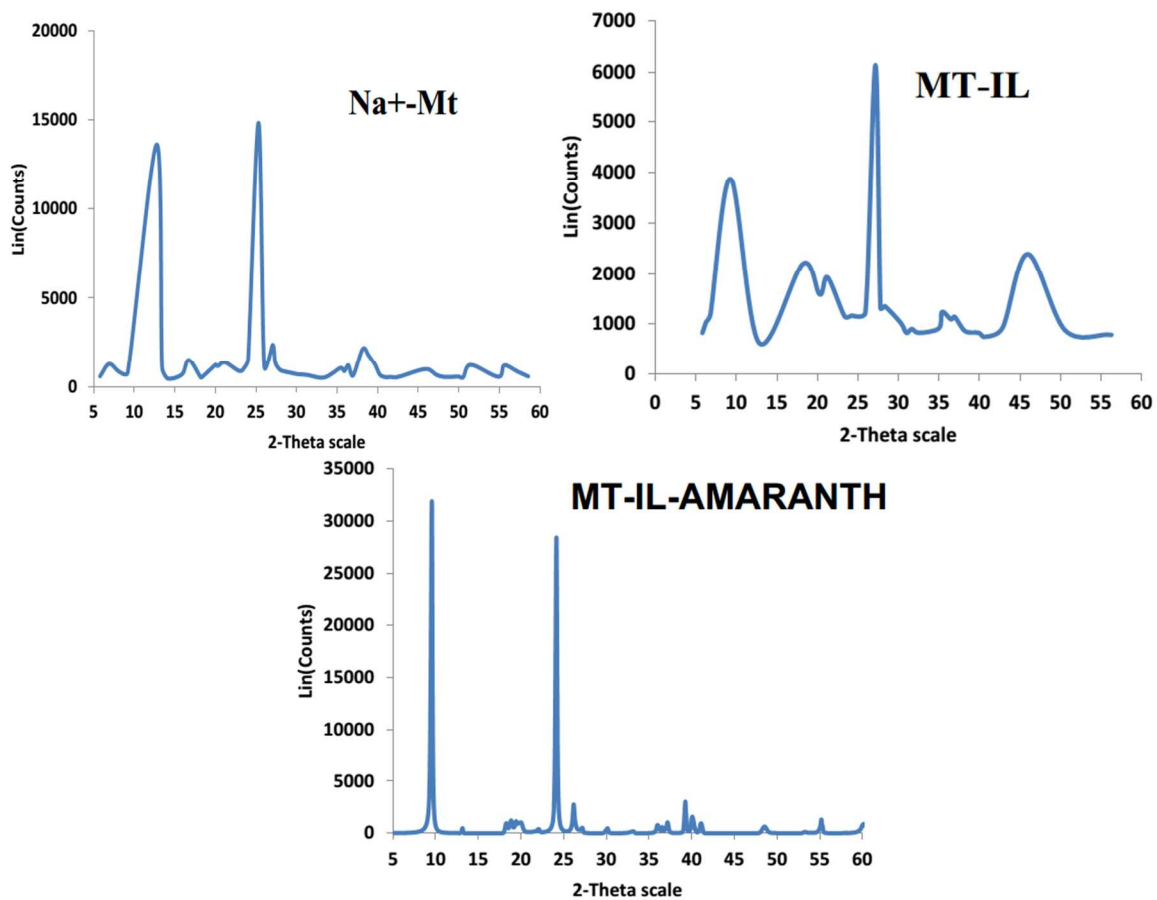


Fig. 1a, 1b and 1c showing the XRD of Na⁺-Mt, Mt-IL and Mt-IL after adsorption of amaranth

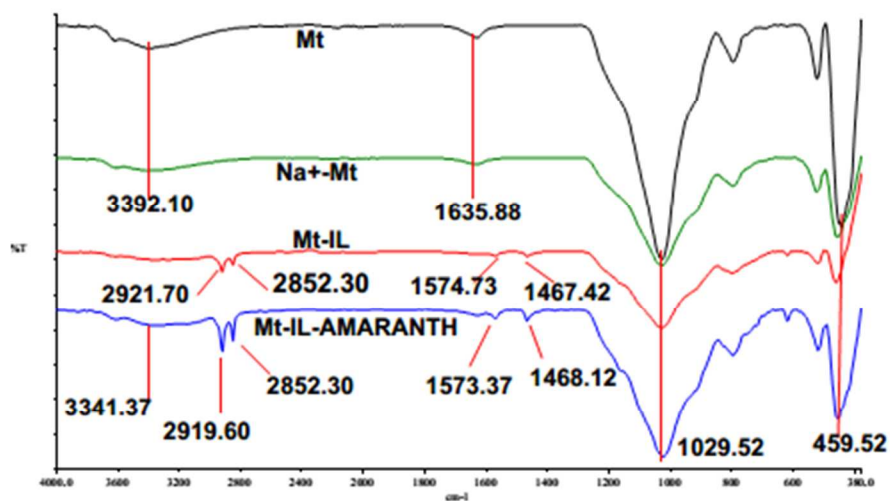


Fig 2. FT-IR spectra of Mt, Na⁺-Mt, Mt-IL and Mt-IL-Amaranth

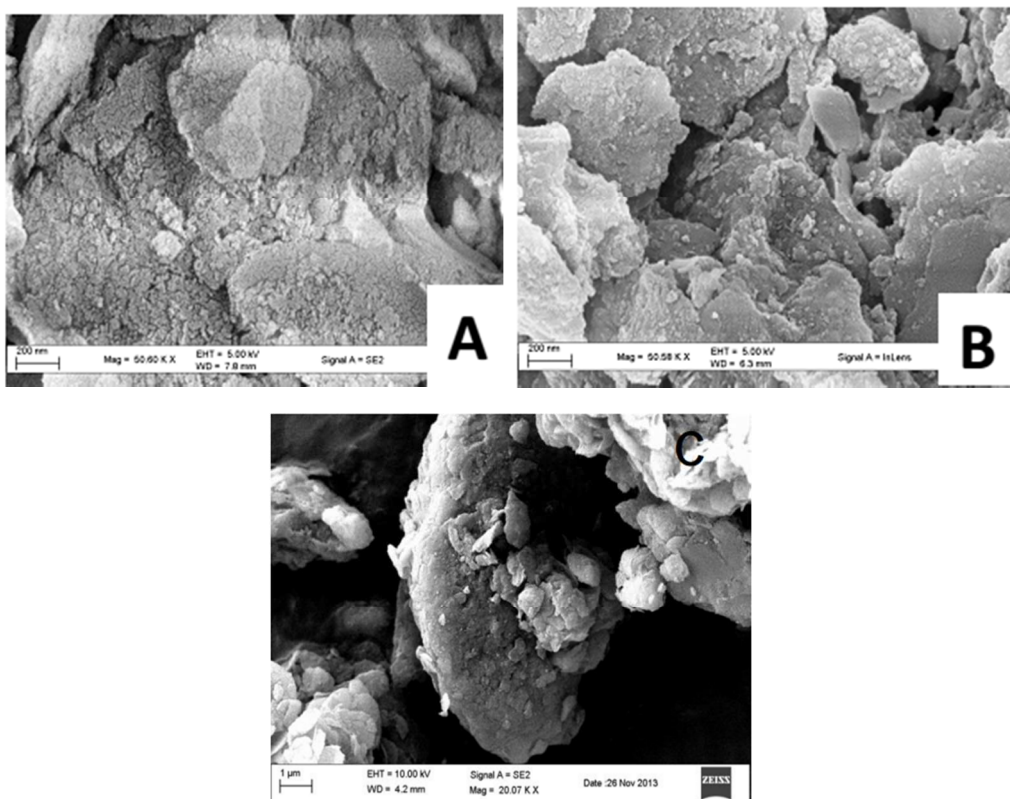


Fig 3. SEM images of Na⁺-Mt (a) and Mt-IL (b) before adsorption and after adsorption (c)

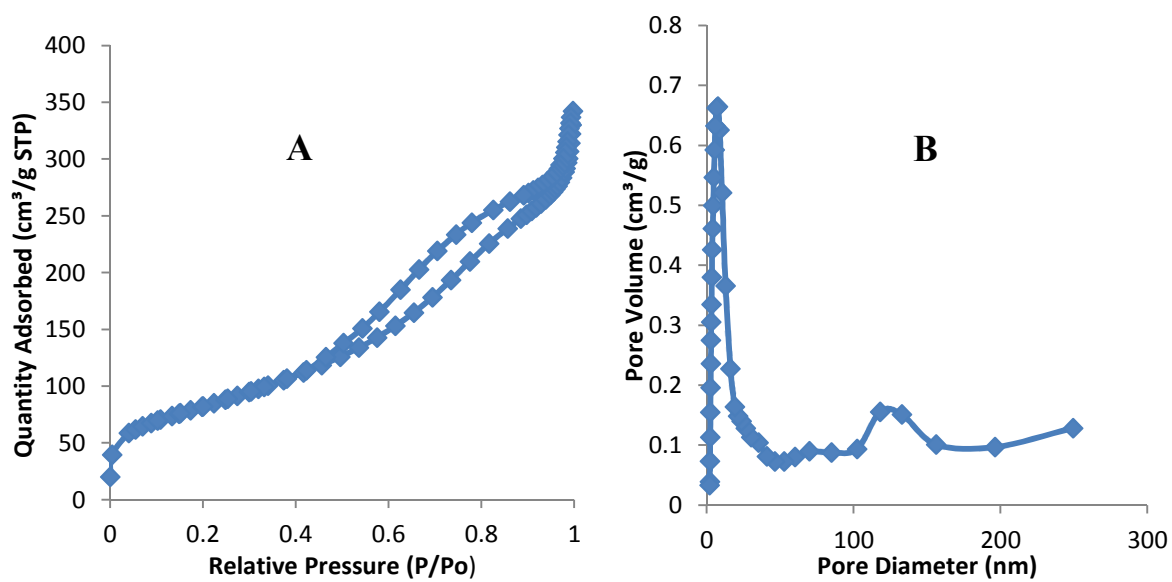


Fig 4a and 4b. N₂ adsorption-desorption isotherm and pore size distribution of Na-Mt respectively.

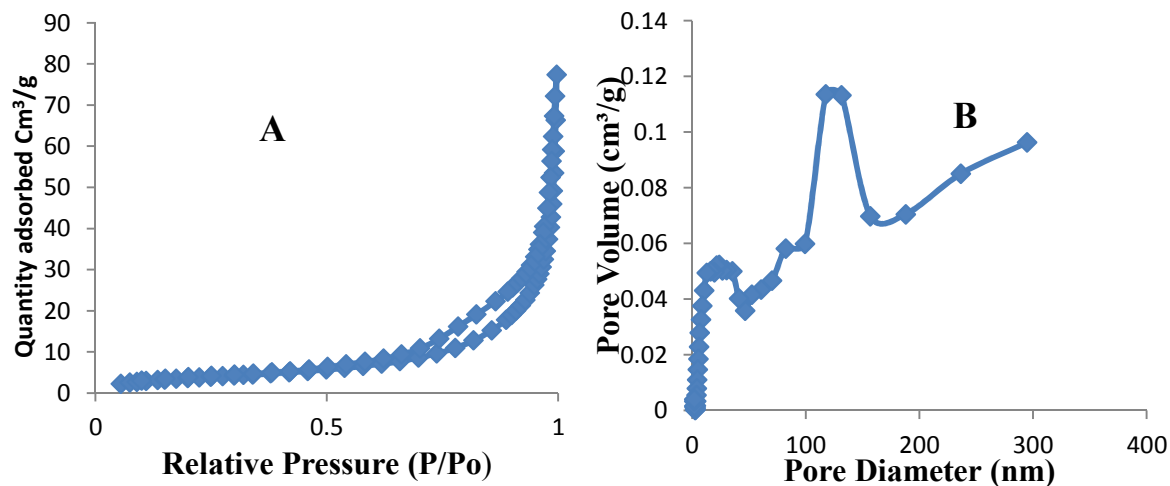


Fig 5a and 5b. N₂ adsorption desorption isotherm and pore size distribution of Mt-IL respectively

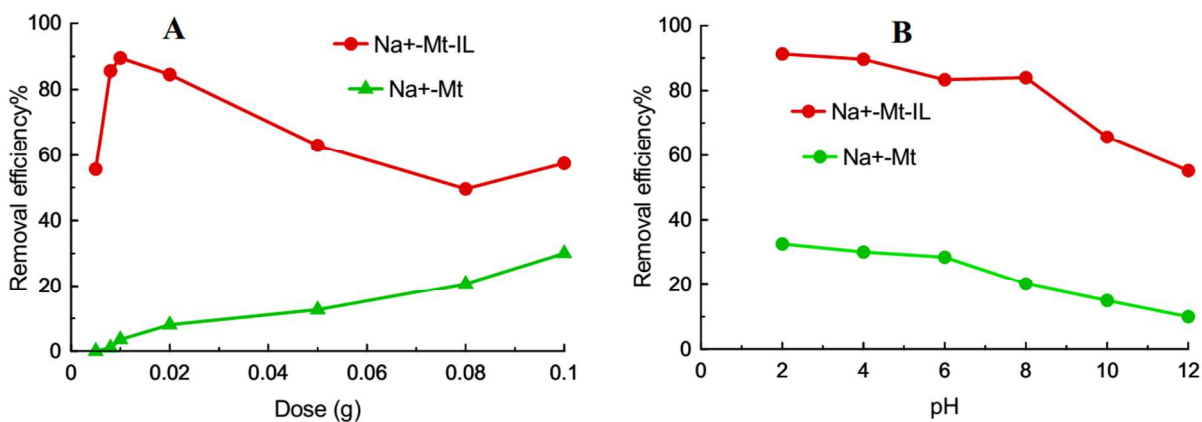


Fig 6a and 6b, showing the effect of dose of adsorbent and pH respectively

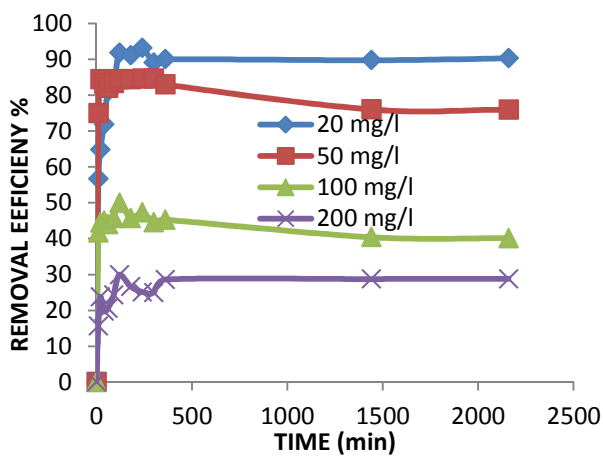


Fig 7. Plot of removal efficiency % against time (min) for four different concentrations at pH 2

Table 3. Experimental values for q_e (mg/L) and parameters for pseudo-first-order, pseudo-second-order and intra-particle diffusion

| Concentrations | Temp | $q_{e,exp}$ (mg/g) | Pseudo-first-order | | | Pseudo-second-order | | | Weber–Morris model | | |
|----------------|-------|-----------------------|-----------------------|----------------|-------|-----------------------|-----------------|-------|--------------------|---------------------------------------|-------|
| | | | $q_{e,cal}$ (mg/g) | k_c (1/h) | R^2 | $q_{e,cal}$ (mg/g) | k (g/mg h) | R^2 | q_e | k_{id} (mg/g/ h ^{1/2}) | R^2 |
| 200 mg/L | 313 k | 239.360 | 6.869 | 0.002 | 0.697 | 222.222 | 0.000 | 0.987 | 142.790 | 4.525 | 0.519 |
| 100 mg/L | | 199.787 | 0.714 | 0.002 | 0.817 | 181.818 | 0.004 | 0.998 | 174.480 | 0.652 | 0.170 |
| 50 mg/L | | 168.853 | 2.115 | 0.004 | 0.157 | 178.571 | 0.003 | 0.999 | 159.710 | 0.566 | 0.278 |
| 20 mg/L | | 73.493 | 3.492 | 0.004 | 0.671 | 74.074 | 0.000 | 0.999 | 47.640 | 1.611 | 0.747 |
| 200 mg/L | 303 k | 224.853 | 4.119 | -0.008 | 0.455 | 196.078 | 0.001 | 0.995 | 255.000 | -2.720 | 0.217 |
| 100 mg/L | | 192.853 | 3.650 | 0.098 | 0.817 | 227.273 | 0.000 | 0.996 | 165.590 | 2.026 | 0.468 |
| 50 mg/L | | 165.440 | 4.268 | 0.004 | 0.768 | 166.667 | 0.001 | 0.999 | 126.030 | 2.454 | 0.721 |
| 20 mg/L | | 60.267 | 3.160 | 0.004 | 0.824 | 60.606 | 0.002 | 0.998 | 41.449 | 1.164 | 0.739 |
| 200 mg/L | 293 k | 246.613 | 5.933 | -0.008 | 0.190 | 238.095 | 0.000 | 0.923 | 194.990 | 3.843 | 0.276 |
| 100 mg/L | | 204.587 | 100.324 | 0.098 | 0.545 | 227.273 | 0.000 | 0.996 | 156.100 | 3.791 | 0.699 |
| 50 mg/L | | 173.973 | 2.883 | 0.005 | 0.912 | 178.571 | 0.003 | 0.999 | 164.810 | 0.757 | 0.651 |
| 20 mg/L | | 60.480 | 4.147 | 0.001 | 0.84 | 66.667 | 0.002 | 0.998 | 50.656 | 0.865 | 0.886 |

Table 4. The q_m and b values in Langmuir equation, the K_f and $1/n$ values in Freundlich equation, q_s and β values in Dubinin–Radushkevich, bT and AT values in Temkin models and their respective correlation coefficients values.

| Temp | Langmuir model | | | Freundlich model | | | Dubinin–Radushkevich model | | | | Temkin model | | |
|-------|-----------------|---------------|-------|------------------|------------------|-------|----------------------------|---|-----------------|-------|-----------------------|----------------|-------|
| | q_m (mg/g) | b (L/mg) | R^2 | K_f (L/mg) | n (-) (g/L) | R^2 | q_m (mol/g) | β (mol ² /kJ ²) | E (kJ/mol) | R^2 | bT (g kJ/mg mol) | AT (L/mg) | R^2 |
| 313 k | 243.902 | 0.0229 | 0.996 | 77.657 | 4.08 | 0.862 | 205.799 | 5×10^{-9} | 10.000 | 0.939 | 75.53 | 8.044 | 0.935 |
| 303 k | 238.095 | 0.099 | 0.995 | 54.435 | 3.25 | 0.654 | 250.711 | 9×10^{-9} | 8.452 | 0.797 | 41.165 | 0.836 | 0.851 |
| 293 k | 263.158 | 0.091 | 0.992 | 59.973 | 3.305 | 0.598 | 250.711 | 8×10^{-9} | 7.906 | 0.831 | 56.875 | 2.302 | 0.861 |

Table 5 Comparison of adsorption capacities of MT-IL with other materials

| pH | Adsorption capacity (mg/g) | Material | Reference |
|------|----------------------------|---|--------------|
| 2 | 10.00 | Alumina reinforced polystyrene | 57 |
| 2 | 14.90 | Peanut hull | 71 |
| 3-9 | 1.05 | Iron oxide nanoparticles coated with cetyltrimethylammonium bromide | 63 |
| 2-11 | 18.80 | Activated carbon | 72 |
| 2 | 100.17 | Activated de-oiled mustard | 73 |
| 3 | 3.44 | Pomegranate peel | 74 |
| 6-12 | 65.04 | Tamarind pod shells | 75 |
| 9 | 95.12 | Activated carbon | 75 |
| 2 | 263.20 | Mt-IL | Present work |
| 2 | 6.00 | Na-Mt | Present work |

Table 6. Thomas model parameters at different concentrations using non-linear regression analysis

| C_0 (mg/L) | v (mL/min) | K_{Th} (mL/min mg ⁻¹) | q_0 (mg/g) | R^2 |
|--------------|--------------|-------------------------------------|--------------|-------|
| 50 | 3.2 | 1.4×10^{-4} | 393.64 | 0.941 |
| 100 | 3.2 | 0.86×10^{-4} | 580.89 | 0.998 |
| 200 | 3.2 | 0.95×10^{-4} | 608.60 | 0.996 |

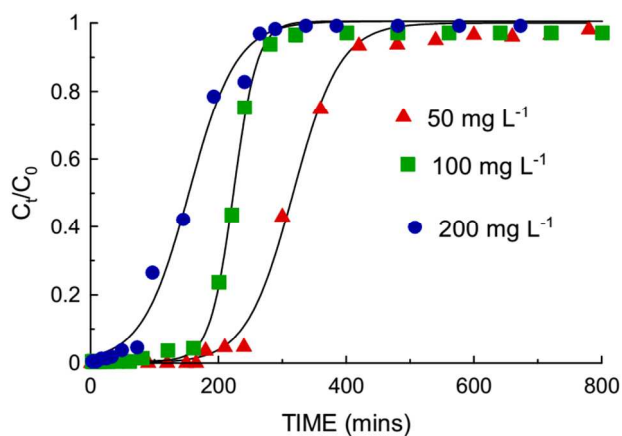
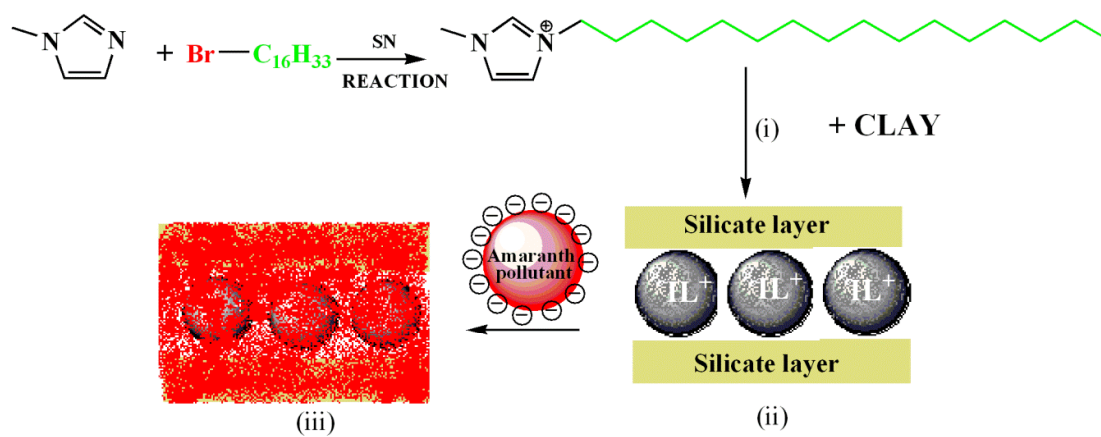


Fig 8. Breakthrough curves showing the effect of influent concentration on amaranth dye

Graphical Abstract



i) Process of intercalating ionic liquid between clay layer

ii) Ionic liquid intercalated between silicate layer of montmorillonite

iii) Amaranth dye on modified montmorillonite after adsorption



1-methyl, 3-decahexyl imidazolium